



Study of stability and aggregation kinetics of coated zero-valent iron nanoparticles

Yongxiang Zhang*, Yuhui Lin, Yajun Li, Wenjing Yang, Yifei Ye, Jinhao Wang

College of Architectural Engineering, Beijing University of Technology, Beijing, China, emails: yxzhang@bjut.edu.cn (Y.X. Zhang), linyh.william@gmail.com (Y.H. Lin), 632974591@qq.com (Y.J. Li), 675576063@qq.com (W.J. Yang), 1271039353@qq.com (Y.F. Ye), 1308009827@qq.com (J.H. Wang)

Received 11 December 2021; Accepted 7 April 2022

ABSTRACT

Sulfidated nanoscale zero-valent iron (S-NZVI) has strong reactivity and electron selectivity and is one of the promising remediation materials in the field of ground water remediation. Due to the easy aggregation of the material, its reactivity is reduced, limiting the application in environmental remediation. In this paper, the zeta potential (ζ) of S-NZVI at different pH and the electrophoretic mobility of S-NZVI coated with sodium alginate (SA-S-NZVI) at different ionic strengths were investigated. The thickness of the polyelectrolyte layer and the surface charge of sodium alginate were also calculated by combining the soft particle theory. The polyelectrolyte layer properties were correlated with the particle dispersion to study the particle properties. The results showed that the thickness of the coating layer increased with the concentration of sodium alginate, and the settling rate and aggregation rate decreased. Thus the stability of the particles increased. Combined with the XDLVO theory, although the polyelectrolyte layer increases the surface potential of S-NZVI and improves the electrostatic repulsion, the spatial effect plays a significant role in the total repulsion energy. The smaller the particle size of SA-S-NZVI, the weaker the magnetism. Therefore, the thicker the polyelectrolyte layer, the better the stability of the particles. Finally, the change of particle size with time was predicted by the Smoluchowski aggregation model. This study has a significant effect on the sedimentation process of water treatment, the problem of filter clogging of drinking water, and the problem of aquifer blockage in the infiltration process of surface water.

Keywords: Nanoscale zero-valent iron; Polyelectrolyte; Soft particle; Dispersion stability; Extended DLVO

1. Introduction

Groundwater is the main drinking water resource in many areas of China. Due to the increase of human production activities, groundwater pollution is becoming more and more serious, so the environmental remediation of groundwater has become an urgent problem. In recent years, nanoscale zero-valent iron (NZVI) has been widely studied because of its unique physical and chemical properties, such as the large surface area to volume ratio and high interfacial reactivity [1–6]. The feasibility of its industrial production

has been demonstrated by researchers who have explored the operational protocols for its industrial preparation [5]. Thus, it shows great potential in the field of groundwater environmental remediation. However, NZVI has the potential for agglomeration, passivation, loss and poor electron selectivity in water, making it still limited for in-situ groundwater remediation and other applications.

Several modification methods have successfully alleviated the problem of reduced NZVI reactivity, such as doping precious metals to form bimetallic nanoparticles [7], loading NZVI with solid carriers to immobilize them

* Corresponding author.

[8,9], covering NZVI particles with protective coating [1,9]. Sulfide modification is a method to passivate the surface of NZVI. A layer of iron sulfide shell (FeS_x) on the surface of the nano zero-valent iron formed core-oxide shell structure. The FeS_x protective layer can effectively prevent the inner NZVI core from oxidizing by the surrounding environmental media [10]. In addition, the presence of off-domain electrons within the FeS_x protective layer facilitates the electron transfer, thus improving the ability of the material to reduce the contaminants, which is an excellent solution to the disadvantage that NZVI is prone to passivation [10,11]. However, due to van der Waals forces and magnetic attraction of zero-valent iron, S-NZVI particles still form agglomerates, which dramatically reduces their transport in contaminated groundwater and soil. Therefore, there is a need to modify S-NZVI particles by introducing repulsive forces that overcome van der Waals forces and magnetic attraction to enhance the stability of S-NZVI and thus its migration in groundwater. In order to solve the problem of particle agglomeration, the modification method of coating particles with polymer electrolytes has received a lot of attention [12]. Asad et al. [13] used carboxymethyl-cellulose coated NZVI to enhance NZVI dispersion for in situ groundwater injection and performed numerical calculations to optimize the injection parameters. Liu et al. [14] demonstrated the feasibility of xanthan gum-coated reduced graphene oxide-based nanoscale zero-valent iron for the in situ remediation of Cr(VI)-contaminated aquifers.

Currently, the dispersion properties of polyelectrolyte-coated NZVI have been studied extensively and the stabilization mechanisms of the particles are analyzed by considering the electrostatic repulsive forces on the particle surface and the spatial forces provided by the polyelectrolyte layer, respectively [15]. But the polyelectrolyte-coated NZVI, which is essentially a composite particle, consists of an internal rigid iron core and a polyelectrolyte layer (PEL) grafted on its surface [16,17]. The polyelectrolyte layer entrains an additional charge and allows ions in solution to penetrate its surface and disperse into the interior, thus significantly changing the charge characteristics of the NZVI surface [18]. Thus, the presence of a polyelectrolyte layer affects both spatial and electrostatic repulsion, so Smoluchowski's theory based on the complex particle hypothesis is not applicable to polyelectrolyte-coated NZVI, and the concept of zeta potential loses its relevance at this point [19,20]. Ohshima argues that polyelectrolyte-coated electrolyte-covered colloidal particles as soft particles, proposed the soft particle theory, and derived an expression for the electrophoretic mobility of such particles under different conditions [16].

At present, the dispersion properties of polyelectrolyte-coated NZVI have been studied extensively and the stability mechanisms of the particles have been analyzed by considering the electrostatic repulsive forces on the particle surface and the spatial forces provided by the polyelectrolyte layer, respectively [15], but few researchers have paid attention to the effect of the polyelectrolyte coating layer on the electrostatic repulsive forces on the surface of the particles. In fact, the polyelectrolyte-coated NZVI is essentially a composite particle consisting of an internal rigid iron core and a polyelectrolyte layer (PEL) grafted on its surface [16,17]. The polyelectrolyte layer carries an additional

charge and allows ions in solution to penetrate the surface and disperse into the interior, thus significantly changing the charge characteristics of the NZVI surface [18]. Thus the presence of the polyelectrolyte layer affects both spatial and electrostatic repulsion, so Smoluchowski's theory based on the complex particle hypothesis is not applicable to polyelectrolyte-coated NZVI, and the concept of zeta potential loses its meaning at this point [19,20]. Ohshima considers that the polyelectrolyte-covered colloidal particles covered by polyelectrolytes are soft particles, proposed the soft particle theory, and derived the expressions for the electrophoretic mobility of such particles under different conditions [16].

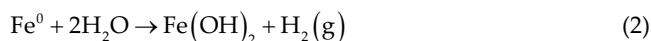
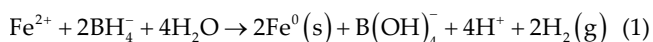
In this paper, S-NZVI is coated with sodium alginate to prevent aggregation and settling and enhance water mobility. The use of anionic polyelectrolytes correlates with the mobility of particles in water since most mineral and natural organic surfaces encountered in, for example, groundwater is negatively charged [21,22]. Therefore, an anionic polyelectrolyte layer can provide electrostatic repulsion from these surfaces to reduce the adhesion phenomenon. Dynamic light scattering (DLS) was used to measure the particle size to calculate the aggregation rate and evaluate the particles' stability in conjunction with the settling experiments. The soft particle theory of Ohshima was used to calculate the surface potential and the thickness of the polyelectrolyte layer of S-NZVI coated with sodium alginate (SA-S-NZVI), and the extended DLVO theory was used to explain the aggregation mechanism of SA-S-NZVI. Finally, the Smoluchowski aggregation kinetic model was used to predict the variation of the mean particle size.

2. Experimental section

2.1. Preparation of sodium alginate coated sulfidated nanoscale zero-valent iron

Sodium alginate and sodium sulfide for the preparation of SA-S-NZVI were purchased from Tianjin Fuchen Chemical Reagent Factory. Ultrapure water (SIM-T30UV, Beijing Fly Seth Technology Co., Ltd., China) was deoxygenated by nitrogen (Beijing Shunchi Donghuan Dry Ice Operation Center, China) before the reaction. All reagents for the experiments were analytically pure, and all solutions and dilutions were prepared in ultrapure water.

S-NZVI was prepared by surface etching method, S^{2-} hydrolysis to produce H^{\ominus} and H_2S had a corrosive effect on NZVI, and the generated Fe^{2+} combined with S^{2-} to produce FeS on the surface of NZVI [23]. NZVI was prepared using the liquid phase reduction method [24,25] by dissolving 2.48 g $\text{FeSO}_4 \cdot 7\text{H}_2\text{O}$ in 350 mL of ultrapure water. 0.68 g of NaBH_4 was dissolved in 150 mL of ultrapure water and then added drop by drop to the above solution. At the same time, the reaction was stirred with an electric mixer (JJ-1, Beijing Zhongxingweiye Instrument Co., Ltd., China) at 600 r min^{-1} , and continued to stir for 15 min after the reaction was completed, and the reaction equation was as in Eq. (1). The mixture was filtered, and the collected solid particles were rinsed twice with deionized water and once with anhydrous ethanol, dried and sealed in a refrigerator for storage. The reaction equation was shown in Eqs. (1) and (6) [26].



The 0.5 g S-NZVI were dispersed in different concentrations of sodium alginate (0.0, 0.1, 0.2, and 0.3 wt.%), sonicated for 30 min, then centrifuged at 27,500 rpm for 80 min. The supernatant was decanted, washed several times with ultrapure water and dried. The samples were recorded as S-NZVI, 0.1% SA-S-NZVI, 0.2% SA-S-NZVI and 0.3% SA-S-NZVI in order.

2.2. Material characterization

S-NZVI was suspended in 1.0 mM NaCl solution, and the pH of the solution was adjusted using NaOH or HCl and sonicated for 30 min in an ultrasonic cell grinder. Zeta potential and particle size analyzer (90Plus Zeta, Brookhaven Instruments Corporation) was used to determine the electrophoretic mobility (u_e) of S-NZVI at different pH in the range of 3 to 10. The zeta potential of S-NZVI was calculated by the Smoluchowski equation: $\zeta = \eta u_e / \epsilon$, where η is the water viscosity and ϵ is the dielectric constant of water. The four samples prepared in section 2.1 were suspended in NaCl solutions of different ionic strengths (5.0, 10.0, 20.0, 40.0, 60.0, 80.0 mM) at pH = 8.0. The electrophoretic mobilities of the samples were measured.

The four samples prepared in section 2.1 were configured into a suspension of 1.0 g L⁻¹ using 1.0 mM NaCl solution at pH = 8.0. The absorbance of Fe was measured at 508 nm using a UV spectrophotometer (2082S UV/VIS, Unico Instrument Corporation) at different times with a scan time of 4,000 s. The scan time was 4,000 s, and the scan interval was 30 s.

The particle size (a_h) of SA-S-NZVI nanoparticles was determined using the dynamic light scattering (DLS) module of a zeta potential and particle size analyzer (90Plus Zeta, Brookhaven Instruments Corporation). The above samples were configured into a suspension of 0.015 g L⁻¹, and the solution was adjusted to pH = 8.0 using NaOH or HCl and measured immediately after sonication in a nitrogen atmosphere for 30 min. A photodetector detected the scattered light at a scattering angle of 90° for 60 s. According to Rayleigh's approximation, the intensity of the scattered light was positively correlated with the sixth power of the particle size, so the intensity distribution was susceptible to the particle size and did not apply to wide distribution samples.

In order to effectively determine the particle-size distribution of agglomerated particles, the intensity-averaged (by intensity) data and the number-averaged (by number) data of DLS were compared. In this paper, the number-averaged hydraulic particle size was chosen to characterize the size distribution of particles.

2.3. Determination of adhesion efficiency

The aggregation kinetics of SA-S-NZVI was characterized by calculating the initial aggregation rate constant (k) and the attachment efficiency (α). The hydrodynamic radius (a_h) was linearly dependent on time t when the aggregation behavior was first started. Therefore, the initial aggregation rate constant can be obtained by performing a linear least squares regression analysis on the amount of variation of $a_h(t)$ with t . This regression analysis is usually performed in the time range from $t = 0$ to the value of $a_h(t)$ reaching $1.25a_h(0)$ [27]. The initial aggregation rate of particles at different ionic strengths was calculated [28].

$$k \propto \frac{1}{N_0} \left(\frac{da_h(t)}{dt} \right)_{t \rightarrow 0} \quad (7)$$

where N_0 is the initial concentration of the nanoparticle suspension (unit: M). The adhesion efficiency α_{pp} reflects the chance of effective collisions between particles. It is defined as the reaction-limited aggregation, so the attachment efficiency ($\alpha_{pp} < 1$) is the same as the diffusion-limited aggregation, which means the attachment efficiency ($\alpha_{pp} = 1$). The ratio of the derived aggregation rates [29]:

$$\alpha_{pp} = \frac{k}{k_{fast}} = \frac{\frac{1}{N_0} \left(\frac{da_h(t)}{dt} \right)_{t \rightarrow 0}}{\frac{1}{N_{0,fast}} \left(\frac{da_h(t)}{dt} \right)_{t \rightarrow 0,fast}} \quad (8)$$

where the subscript "fast" refers to diffusion-limited aggregation. k_{fast} takes the average value of k under the diffusion-limited aggregation stage.

3. Theoretical model

3.1. Calculation of polyelectrolytic layer thickness

Since the anions and charges in the solution can pass through the encapsulated S-NZVI surface and be distributed inside the adsorbed layer, the electrophoretic mobility was measured in combination with Ohshima's soft particle theory to determine the properties of the polyelectrolyte adsorbed layer. According to Ohshima, the electric potential around the soft particles consists of the Donnan potential (ψ_{DON}) with thickness d inside the adsorbed layer and the adsorbed layer with surface potential (ψ_0) at the boundary of the solution [19,20,30] (Fig. 1). Combining the Navier-Stokes equation to calculate the friction of the adsorbed layer, the expression for the electrophoretic mobility of soft particles is [31].

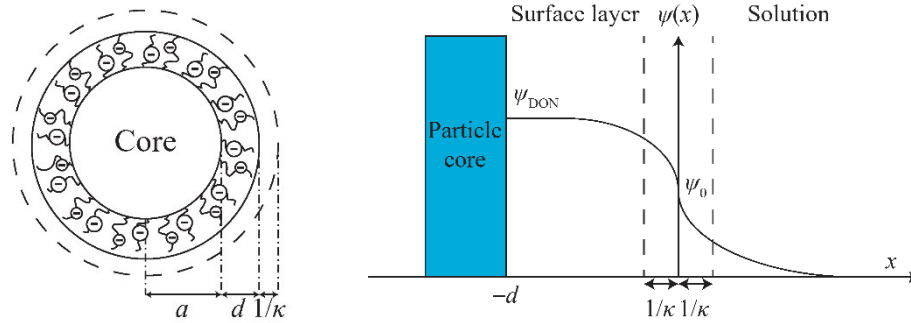


Fig. 1. Schematic of the potential distribution across the surface of change layer [18].

$$\Psi_{DON} = \frac{k_B T}{ze_0} \ln \left[\frac{ZN}{2zn} + \left\{ \left(\frac{ZN}{2zn} \right)^2 + 1 \right\}^{1/2} \right] \quad (9)$$

$$\Psi_0 = \Psi_{DON} - \frac{k_B T}{ze_0} \tanh \frac{ze_0 \Psi_{DON}}{2k_B T} + \frac{4k_B T}{ze_0} \cdot e^{-\kappa_m d} \cdot \tanh \frac{ze_0 \zeta}{4k_B T} \quad (10)$$

$$\kappa = \sqrt{\frac{2nz^2 e_0^2}{\epsilon k_B T}} \quad (11)$$

$$\kappa_m = \kappa \cosh \left(\frac{ze_0 \Psi_{DON}}{k_B T} \right) \quad (12)$$

$$u_e = \frac{\epsilon}{\eta} \cdot \frac{\Psi_0 / \kappa_m + \Psi_{DON} / \lambda}{1 / \kappa_m + 1 / \lambda} \cdot \frac{2}{3} \cdot \left[1 + \frac{1}{2(1 + d/a)^3} \right] + \frac{Ze_0 N}{\eta \lambda^2} + \frac{8\epsilon k_B T}{\eta \lambda ze_0} \cdot \tanh \frac{ze_0 \zeta}{4k_B T} \cdot \frac{e^{-\lambda d} / \lambda - e^{-\kappa_m d} / \kappa_m}{1 / \lambda^2 - 1 / \kappa_m^2} \quad (13)$$

where, ϵ (unit: $C^2 J^{-1} m^{-1}$) is the dielectric constant of water; Z (unit: M) is the valence of the ionization group of the polyelectrolyte; N is the concentration of the polyelectrolyte in the coating layer; z is the valence of the electrolyte in the aqueous phase (NaCl is used in this paper, z is taken as 1); n (unit: M) is the concentration of the electrolyte; e_0 (unit: C) is the electronic charge; k_B (unit: $J K^{-1}$) is the Boltzmann constant; κ (unit: m^{-1}) is the Debye constant, which is the reciprocal of the electrostatic shielding distance; a and d (unit: m) are the particle size and the thickness of the coating layer, respectively; ζ (unit: V) is the zeta potential of bare S-NZVI; λ (unit: m^{-1}) is related to the parameter γ (unit: $N s m^{-3}$) of the coefficient of friction of the liquid flowing around the polymer as a parameter fit. $1/\lambda$ can indicate the softness of the polyelectrolyte layer, and when $1/\lambda \rightarrow 0$, the coating layer is rigid, at which time Eq. (13) is equivalent to the Smoluchowski equation. The electrophoretic mobilities of bare S-NZVI and encapsulated S-NZVI at different ionic strengths were measured and used to fit the calculated Eqs. (9), (10) and (13) to obtain N , λ and d .

3.2. Aggregation kinetic model

Von Smoluchowski proposed the aggregation kinetic equation in 1917 [32], which mathematically reflects the aggregation process of particles of different particle sizes in the aggregation process under the simplified conditions of ignoring the assumptions of gravity, no floc splitting, no medium flow, and flocs colliding with each other along a straight line in the context of colloid chemistry.

$$\frac{dn_k}{dt} = \frac{1}{2} \alpha_{pp} \sum_{i+j=k} \beta(i, j) n_i n_j - \alpha_{pp} n_k \sum_{i=1}^z \beta(i, k) n_i \quad (14)$$

where the subscripts represent the number of primary particles consumed to form aggregates of the corresponding order, corresponding to n_i, n_j, n_k (unit: m^{-3}) are the concentrations of aggregates of the corresponding order; z is the number of primary particles consumed to form the largest flocs among them (i, j, k, z); α_{pp} denotes the collision efficiency calculated by Eq. (8); β (unit: $m^3 s^{-1}$) is a function related to the volume of two colliding particles. The first term on the right-hand side of the equation indicates the rate at which a cluster of order i and a cluster of order j collide to form a cluster of order k , and the second-term indicates the rate at which a cluster of order k is lost upon collision with another cluster. The $1/2$ before the first term ensures that the same collisions are not counted twice in the summation process. The equation defines the rate of change of the k -th order agglomerate concentration. Details about the theory and calculations can be found in the SI.

4. Results and discussion

4.1. Effect of pH on the zeta potential of S-NZVI particles

As shown in Fig. 2, the zeta potential of bare S-NZVI is positive under acidic conditions and negative under alkaline conditions, and the isoelectric point is around $pH = 7.0$ when the electrostatic force on the particle surface becomes smaller, and the repulsive force is weakened. Since the pH range of groundwater is usually between 6.5 and 8.5, the aggregation rate of bare S-NZVI colloids in this environment is faster and more likely to destabilize and settle. To simulate the groundwater environment, the $pH = 8.0$ was adjusted so that the surface of iron sulfide nanoparticles in this study was negatively charged.

4.2. Stability of SA-S-NZVI sedimentation rate by different coating ratios

Nanoparticles are subject to both diffusion and gravitational sedimentation in the water, and if the diffusion of nanoparticles overcomes the sedimentation, the nanoparticles can remain stable. The gravitational effect is proportional to the square of the particle radius, and the diffusion effect is inversely proportional to the particle size. When the nanoparticles are aggregated into micron-sized clusters, the cluster destabilizes and settles because the diffusion effect is smaller than the settling effect, resulting in a decrease in absorbance. Therefore, the sedimentation rate is expressed as the slope of absorbance vs. time.

As shown in Fig. 3, the dashed line t_0 divides the sedimentation curve into two parts S1, S2 with the slope -1 as the boundary. The settling pattern of bare S-NZVI and SA-S-NZVI settling is similar. Both can be divided into two stages according to S1, S2: In the S1 stage, there are a large

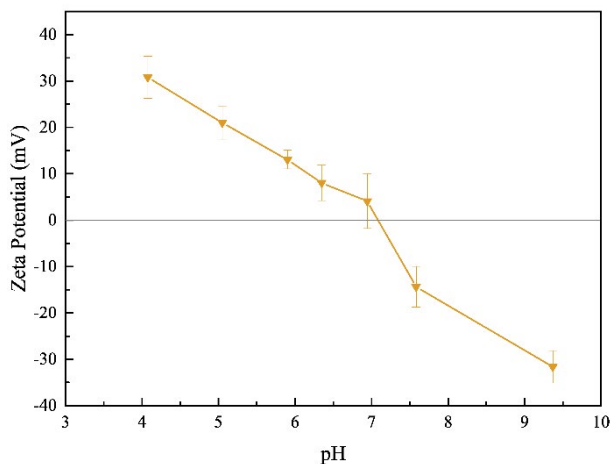


Fig. 2. The zeta potentials of S-NZVI under different pH conditions.

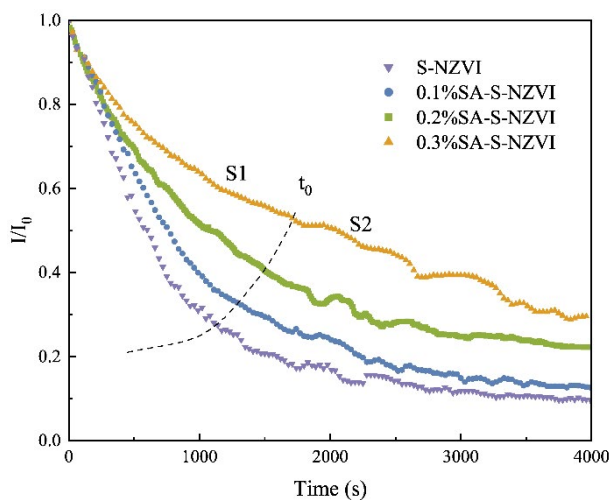


Fig. 3. Settling curves of S-NZVI with different coating ratios.

number of particles exceeding the critical size in the sample, so the settling is rapid. At the moment of t_0 , the settling of most of the large particles is completed, and the settling rate decreases and the sample enters the S2 slow settling stage, which gradually becomes stable.

For SA-S-NZVI, the settling rate of the encapsulated sodium meter iron sulfide was negatively correlated with the concentration of sodium alginate due to the presence of the polyelectrolyte layer. The greater the concentration of sodium alginate, the lower the settling rate in the S1 phase, and the greater the number of particles kept in suspension in the S2 phase, the better the particle stability.

To further study the suspended particles in the aqueous solution after settling and stabilization, the supernatants of the above four freshly prepared suspensions were taken after standing for 2 h. The size distribution of the particles was determined by DLS as shown in Fig. 4. The particle sizes of the three encapsulated S-NZVI that remained suspended after 2 h settling was mainly below 30 nm, with 0.2% SA-S-NZVI being slightly larger and concentrated around 20 nm, and 0.1% SA-S-NZVI and 0.3% SA-S-NZVI being smaller and concentrated around 8 and 10 nm, respectively. It should be noted that S-NZVI was not detected after resting due to the low concentration of suspended matter in the supernatant. This indicates that the polyelectrolyte layer enhances the dispersion of small-sized particles below 30 nm in aqueous solution, but helps weakly in the dispersion of large-sized particles above 30 nm.

4.3. Effect of ionic strength on the stability of SA-S-NZVI

The stability of nanoparticles in an aqueous solution depends to a large extent on the ionic strength. The effect of ionic strength on the stability of SA-S-NZVI in water (pH = 8.0 0.1) was investigated. The adhesion efficiency between the particles was calculated by eq. (8).

The experimental results are shown in Fig. 5. The adhesion efficiency of SA-S-NZVI and bare S-NZVI with different coating ratios increased with the increase of ionic strength in the range of 0.05 mM. The increase of ionic

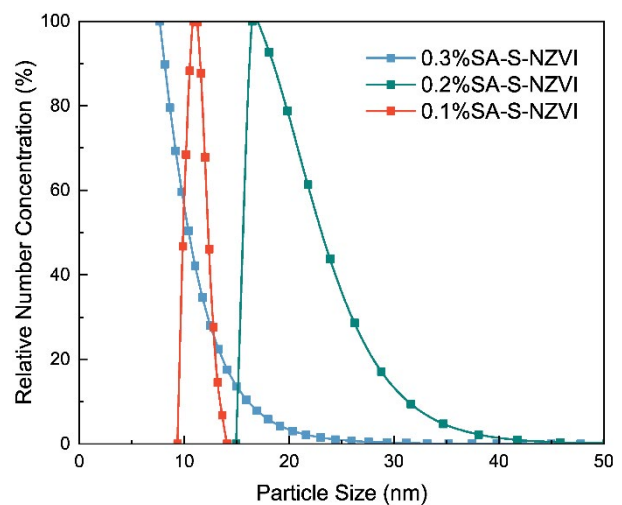


Fig. 4. Particle-size distribution after 2 h of settling.

strength would improve the degree of charge shielding thus the aggregation rate, which was reflected in the increase of adhesion efficiency. In this process, the adhesion efficiency is positively correlated with the amount of NaCl dosed, and this aggregation process is called reaction-limited aggregation ($\alpha < 1$). When the NaCl concentration is greater than 0.05 mM, the charge of SA-NZVI is completely shielded and the potential barrier disappears. The particles undergo diffusion-limited aggregation ($\alpha = 1$) in this process, and the aggregation rate reaches the maximum. The critical concentrations of S-NZVI with different coating ratios of ionic strength were all around 0.05–0.06 mM. The coating ratio has little effect on the adhesion efficiency under different ionic strength conditions.

4.4. Characteristics of the polyelectrolyte coating layer

The magnitude and range of action of the intraparticle spatial repulsion are related to the concentration of polymer adsorbed on the surface, and the thickness of the polyelectrolyte layer [33]. The variation of electrophoretic mobility with ionic strength for S-NZVI with different polyelectrolyte ratios is shown in Fig. 6, where the curves were obtained by fitting the measured average electrophoretic mobility Eqs. (9), (10) and (13), and the parameters are shown in Table 1.

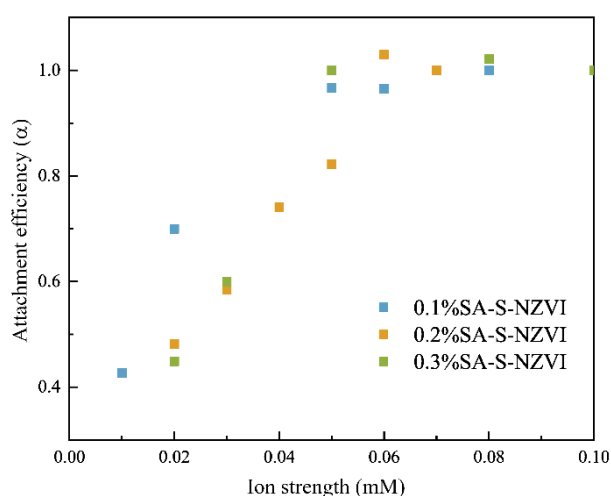


Fig. 5. Effect of ionic strength on the attachment efficiency of S-NZVI with different coating ratios.

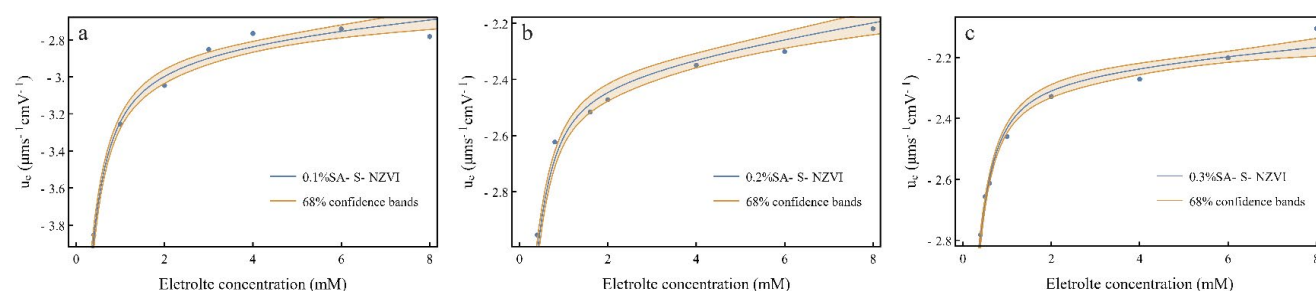


Fig. 6. Effect of ionic strength on the electrophoretic mobility of SA-S-NZVI.

Due to the presence of the polyelectrolyte layer, the diffusion layer around SA-S-NZVI was compressed, and its electrophoretic mobility varied less with the ionic strength than that of bare S-NZVI. The electrophoretic mobility of bare S-NZVI gradually tends to zero with increasing ionic strength, while the electrophoretic mobility of SA-S-NZVI with different coating ratios (0.1%, 0.2%, 0.3%) tends to -2.8 , -2.2 and $-2.3 \mu\text{m s}^{-1} \text{cm V}^{-1}$.

Since the electrophoretic mobility of soft particles is not sensitive to the position of the slipping plane [34], the zeta potential cannot approximate the surface potential of soft particles, and the zeta potential loses its meaning. Therefore, soft particles do not apply to the conventional DLVO theory of the double layer equation to calculate the electrostatic repulsion.

The volume fraction of polyelectrolyte adsorbed onto the NZVI surface was estimated from the calculated average polyelectrolyte layer thickness of the particles and the adsorption concentration.

$$\phi_p = \frac{\Gamma \cdot 4\pi a^2}{\rho_p \cdot \frac{4}{3}\pi[(d+a)^3 - a^3]} = \frac{3 \cdot \Gamma a^2}{\rho_p [(d+a)^3 - a^3]} \quad (15)$$

where, ρ_p ($1.59 \times 10^6 \text{ g m}^{-3}$) is the polyelectrolyte density; d is the thickness of the polyelectrolyte layer; a is the particle radius; and the adsorption amount per unit area is expressed by Γ (unit: g m^{-2}).

4.5. Particle interaction energy calculation based on DLVO theory

The stability of bare S-NZVI particles in solution can be explained by the DLVO theory [35,36]. According to the classical DLVO theory, the primary attraction energy between particles comes from the van der Waals force

Table 1
Calculation of the properties of adsorbed polyelectrolyte layer at pH 8.0 ± 0.1 using Ohshima soft particle theory

Sample	ZN/N_A (mol m^{-3})	d (nm)	$1/\lambda$ (nm)	ϕ_p (10^{-3})
0.1% SA-S-NZVI	3.28 ± 1.08	7.97 ± 4.11	6.63 ± 0.58	113
0.2% SA-S-NZVI	1.47 ± 1.25	10.94 ± 4.68	8.51 ± 1.06	80
0.3% SA-S-NZVI	1.50 ± 1.39	16.62 ± 4.58	9.57 ± 1.97	54

(V_{vdw}), and the repulsion energy depends mainly on the electrostatic double-layer interaction. The magnitude of the potential energy of van der Waals forces between spherical particles is [36]:

$$V_{vdw}(s) = -\frac{A}{6} \left\{ \frac{2a^2}{s(4a+s)} + \frac{2a^2}{(2a+s)^2} + \ln \left[\frac{s(4a+s)}{(2a+s)^2} \right] \right\} \quad (16)$$

where A is Hamaker's constant, which is taken as 10^{-19} J; s is the distance between particle surfaces, and a is the particle radius. In the electrolyte solution, when two charged particles approach each other, their diffuse double layers overlap. If the particles are similarly charged, they will be repelled during the approach. Depending on the particle size and the thickness of the double layer, the equation for the double layer interaction (V_R) is calculated as follows [36–39]:

$$V_{Rs}(s) = \begin{cases} 4\pi\epsilon\psi^2 \cdot \frac{a_1 a_2}{a_1 + a_2} \cdot \ln[1 + \exp(-\kappa s)], & \kappa a \geq 5 \\ 4\pi\epsilon Y_1 Y_2 a_1 a_2 \cdot \left(\frac{k_B T}{e_0}\right)^2 \cdot \frac{\exp(-\kappa s)}{a_1 + a_2 + s}, & \kappa a < 5 \end{cases} \quad (17)$$

$$Y_1 = \frac{8 \tanh[e_0 \psi / (4k_B T)]}{1 + \sqrt{1 - \frac{2\kappa a_i + 1}{(\kappa a_i + 1)^2} \tanh^2[e_0 \psi / (4k_B T)]}} \quad (18)$$

$$\kappa = \sqrt{\frac{1,000 e_0^2 N_A I z_i^2}{\epsilon k_B T}} \quad (19)$$

where ϵ is the dielectric constant of water, ψ is the surface potential, bare S-NZVI is replaced by zeta potential [40–42]. k_B (unit: J K⁻¹) is the Boltzmann constant, T (unit: K) is the absolute temperature, κ (unit: m⁻¹) is the reciprocal of the Debye length, I is the ionic strength (unit: M), e_0 is the charge of a single electron (unit: C), N_A is Avogadro's constant, and since there are only S-NZVI particles in the system, $a_1 = a_2$, $Y_1 = Y_2$.

Since S-NZVI is magnetic, the measured hysteresis line (VSM, Lake Shore Cryotrons' Incorporation) of S-NZVI is shown in Fig. 7 with a saturation magnetization strength of 1,410.62 kA m⁻¹, a coercivity magnitude of 20.49 A m⁻¹, and a residual magnetization strength of 120.08 kA m⁻¹. Therefore, the stability of S-NZVI stability in the aqueous phase is influenced by the interaction between its intrinsic magnetic moments, which attract each other due to the NZVI's magnetic moments even without external magnetic field interference [43]. The effect of the magnetic properties of S-NZVI on its aggregation behavior is expressed in terms of the magnetic potential energy V_M :

$$V_M(s) = \frac{-8\pi\mu_0 M^2 a^3}{9(s/a+2)^3} \quad (20)$$

where μ_0 ($4\pi \times 10^{-7}$ H m⁻¹) is the magnetic permeability in vacuum; M (unit: A m⁻¹) is the magnetization strength.

The interaction of uncoated S-NZVI is shown in Fig. 8, where V_T is the sum of interaction potentials. Assuming an average particle radius is 50 nm. The interaction force is dominated by magnetic force, and there is no energy barrier to prevent the particles from aggregating, and the particles agglomerate rapidly, which is consistent with the observed experimental phenomenon.

When the sodium alginate layer coats S-NZVI, the ions in the solution can penetrate the coating layer and disperse inside, suppose the polyelectrolyte layer is uniformly charged and let Z and N be the valence and concentration of charged groups in the polyelectrolyte layer, respectively, then the electrostatic potential between SA-S-NZVI is [19,33,44].

$$V_{Rs}(s) = \frac{2\pi a \rho_{fix}^2 \sinh^2(\kappa d)}{\epsilon_0 \epsilon_r \kappa^4} \ln \left[\frac{1}{1 - \exp(-\kappa s)} \right] \quad (21)$$

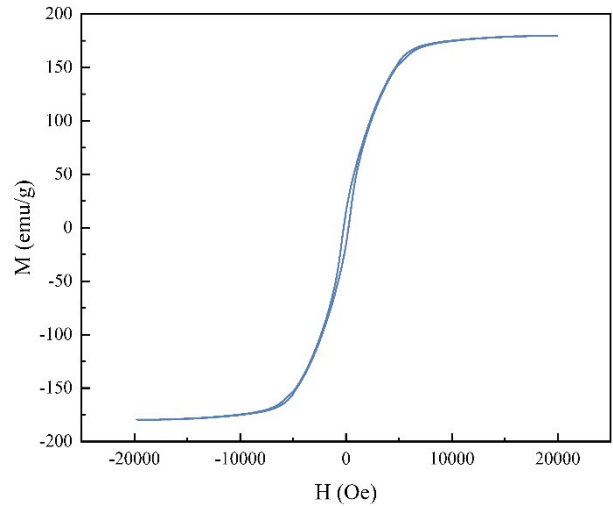


Fig. 7. Hysteresis line of S-NZVI at 298.0 K.

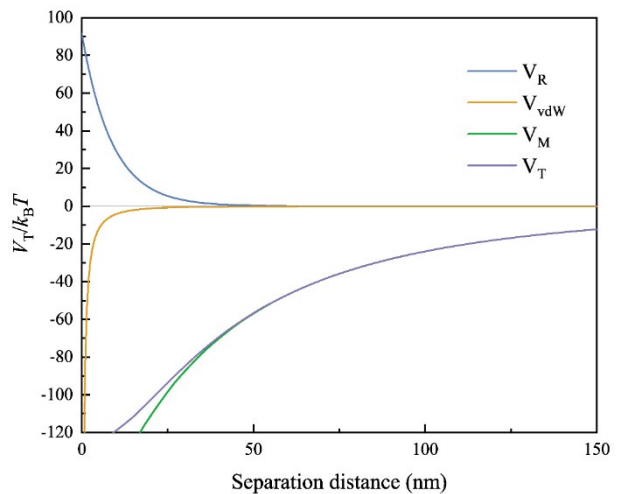


Fig. 8. XDLVO interaction energy curve of S-NZVI.

$$\rho_{\text{fix}} = Ze_0N \tag{22}$$

Meanwhile, according to Donnan equilibrium, the polymer segments in the polyelectrolyte layer are adsorbed and fixed on the particle surface. At the same time, the ions in the solution are free to move, so there is an additional osmotic pressure near the polyelectrolyte layer. When the particle spacing decreases, the polyelectrolyte layers gradually overlap each other increasing the local electrolyte concentration, which increases the osmotic pressure generating osmotic repulsion (V_{osm}) [45,46]. In addition, when the distance between particles is less than d , part of the polymer segment is compressed, leading to a decrease in conformational entropy, which generates elastic repulsion (V_{elas}) [46,47]:

$$V_{\text{Rs}}(s) = \begin{cases} 4\pi\epsilon\psi^2 \cdot \frac{a_1 a_2}{a_1 + a_2} \cdot \ln[1 + \exp(-\kappa s)], & \kappa a \geq 5 \\ 4\pi\epsilon Y_1 Y_2 a_1 a_2 \cdot \left(\frac{k_B T}{e_0}\right)^2 \cdot \frac{\exp(-\kappa s)}{a_1 + a_2 + s}, & \kappa a < 5 \end{cases} \tag{23}$$

$$V_{\text{osm}}(s) = \begin{cases} 0 & 2d \leq s \\ \frac{4\pi a}{v_1} \cdot \phi_p^2 \cdot \left(\frac{1}{2} - \chi\right) \left(d - \frac{s}{2}\right)^2 & d \leq s < 2d \\ \frac{4\pi a}{v_1} \cdot \phi_p^2 \cdot \left(\frac{1}{2} - \chi\right) d^2 \left[\frac{s}{2d} - \frac{1}{4} - \ln\left(\frac{s}{d}\right)\right] & s < d \end{cases} \tag{24}$$

$$V_{\text{elas}}(s) = \begin{cases} 0, & d \leq s \\ \left\{ \frac{2\pi a}{M_w} \cdot \phi_p d^2 \rho_p \right\} \left\{ \begin{aligned} &\frac{s}{d} \ln \left[\frac{s}{d} \left(\frac{3-s/d}{2} \right)^2 \right] \\ &-6 \ln \left(\frac{3-s/d}{2} \right) + 3 \left(1 + \frac{s^2}{d} \right) \end{aligned} \right\}, & s < d \end{cases} \tag{25}$$

where χ (0.45) is the Flory–Huggins constant; ϕ_p is the volume fraction of the poly-electrolyte layer; d is the thickness of the polyelectrolyte layer; v_1 is the volume of the solvent molecules (in this paper, water molecules in m^3); M_w ($1.40 \times 10^7 \text{ g mol}^{-1}$) is the molecular weight of the poly-electrolyte; ρ_p ($1.59 \times 10^6 \text{ g m}^{-3}$) is the density of the polyelectrolyte. In summary, the total interaction energy of the encapsulated S-NZVI is:

$$V_T = V_{\text{vdW}} + V_{\text{Rs}} + V_{\text{osm}} + V_{\text{elas}} + V_M \tag{26}$$

The interaction potentials of SA-S-NZVI are shown in Fig. 9. The main repulsive forces in the system are spatial repulsion ($V_{\text{osm}}, V_{\text{elas}}$) when viewed at a short distance from 0 to $2d$. In contrast, the surface potential of SA-S-NZVI particles (V_{Rs}) is slightly larger than the electrostatic interaction of uncoated S-NZVI (V_R) due to the presence of the polyelectrolyte layer but still cannot resist the attraction of

S-NZVI’s magnetic moment. When the SA-S-NZVI approach distance is less than $2d$, the permeability repulsion generates a great energy barrier, which prevents the further approach of SA-S-NZVI. Let $dV_T/ds = 0$ to find the potential energy trap of 0.3% SA-S-NZVI located at 31.10 nm, which is $-79.93 k_B T$. In summary, the electrostatic repulsion in 1.0 mM electrolyte solution cannot resist the magnetic attraction, and the main repulsion of particles comes from the spatial force. The depth of the potential energy trap can be significantly reduced by increasing the layer thickness. In contrast to the uncoated S-NZVI, SA-S-NZVI with different polyelectrolyte ratios should form loose agglomerates with particle spacing of about 31 nm instead of the dense agglomerates of bare S-NZVI.

Since the adhesion efficiency of SA-S-NZVI increased with the ionic strength, the particle interaction was strongly influenced by the ionic strength. Taking 0.3% SA-S-NZVI as an example, the interaction force between SA-S-NZVI at 0.0–1.0 mM is shown in Fig. 10. The magnitude and range of action of electrostatic repulsion at 0.0–0.5 mM decreases with the increase of ionic strength (Fig. 11), which is reflected in the rapid decay of potential energy trap from $-85.13 k_B T$ (100.00 mM) to -0.07 (0.01 mM) almost disappears. As the electrolyte concentration increases ($<0.5 \text{ mM}$), the change in the depth of the potential energy trap is smaller (purple region). The effect of electrostatic repulsion on the total potential energy becomes minimal. The total potential energy of the particles is dominated by permeation repulsion and magnetic force. The minimum potential energy trap is maintained at about $-85.13 k_B T$, and the effect of ionic strength is negligible. Meanwhile, the physical meaning of the adhesion efficiency is the chance of effective collision between particles, so the critical coagulation concentration (CCC) of particle aggregation can be expressed by DLVO theory as the depth of potential energy trap is greater than the energy of Brownian motion ($1.5 k_B T$). For the attachment efficiency (α_{pp}) to reach 100% the total potential energy equation is given by:

$$\begin{cases} V_T(s) \geq -1.5k_B T \\ \frac{dV_T(s)}{ds} = 0 \end{cases} \tag{27}$$

The critical aggregation concentration of SA-S-NZVI with different coating ratios was $4.53 \times 10^{-2} \text{ mM}$, $3.68 \times 10^{-2} \text{ mM}$, and $4.47 \times 10^{-2} \text{ mM}$, respectively. The particle-size distribution of the samples at the moment of t_0 was measured by the dynamic light scattering method, and the change of the average particle size with time was calculated by taking into Eq. (14).

The initial particle-size distribution of SA-S-NZVI with different cladding ratios, such as the mean particle size as a function of time, is shown in Fig. 12, where the scatter points are the experimentally measured values. The mean particle size of SA-S-NZVI increased by about 133, 114 and 110 nm for the three cladding ratios, respectively, and the curves were calculated by Smoluchowski aggregation model with the coefficients of determination of 0.82, 0.72 and 0.84, respectively, which could predict the experimental results better.

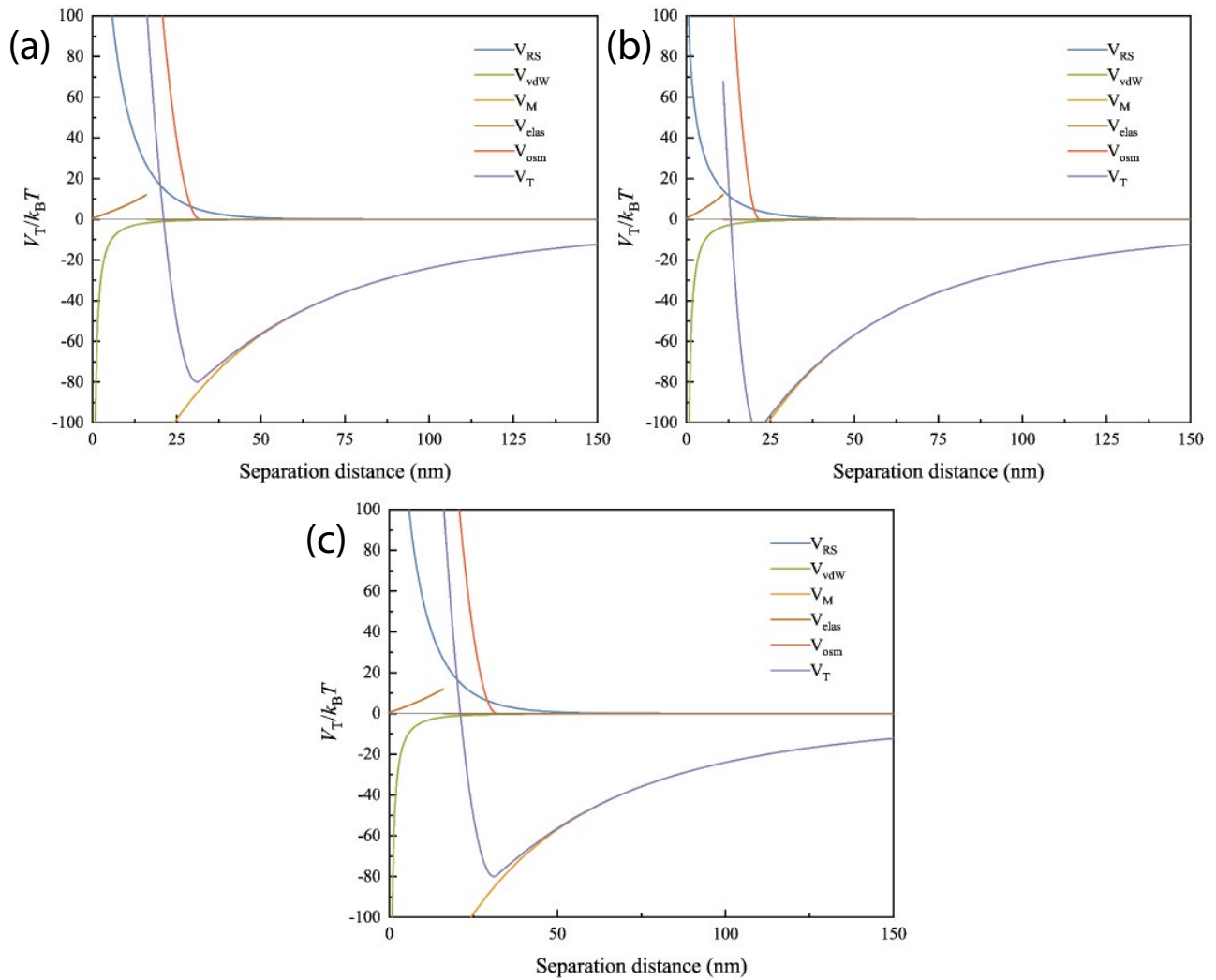


Fig. 9. Particle interaction energy curves for (a) 0.1% SA-S-NZVI, (b) 0.2% SA-S-NZVI and (c) 0.3% SA-S-NZVI.

To further investigate the aggregation mechanism of SA-S-NZVI, the long-range attraction of S-NZVI was considered to be mainly magnetic. In contrast, the magnetic potential energy calculated by Eq. (20) was positively correlated with the sixth power of particle size, and the S-NZVI samples were widely distributed. Therefore, the total potential energy of particles with different particle sizes is significantly different. The variation of particle size and particle spacing on the total potential energy (V_T) is shown in Fig. 13. Since the magnetism is sensitive to particle size, the depth of the potential energy trap slips rapidly with increasing particle size between 30 and 50 nm, and the position of the potential energy trap varies less with particle size. The depth of the potential energy trap for SA-S-NZVI particles below 30 nm is below $-0.82 k_B T$, which is smaller than the energy of colloidal Brownian motion ($1.5 k_B T$). Therefore, the aggregates formed by SA-S-NZVI under this condition are unstable. Thus suspended particles smaller than 30 nm are more likely to remain dispersed in solution, which is consistent with the phenomenon observed in Fig. 4.

5. Conclusion

In this paper, the effect of the polyelectrolyte coating on the electrostatic repulsive force on the particle surface is considered in conjunction with Oshima's theory of soft particles. The role of different coating ratios and ionic strength on the stability of bare and coated S-NZVI was investigated. The results showed that the higher the concentration of sodium alginate, the slower the settling rate. The higher the ionic strength, the higher the adhesion efficiency, and the ionic strength had a more negligible effect on the different coating ratios. And a model was established based on the experimental results to calculate the agglomeration rate of SA-S-NZVI, which was in good agreement with the agglomeration experiment results. In addition, the thickness of the polyelectrolyte layer was 7.97, 10.94 and 16.62 nm for different coating ratios calculated by the soft particle theory. The higher the concentration of sodium alginate, the greater the thickness of the polyelectrolyte layer. Further study with XDLVO theory revealed that the particles always tend

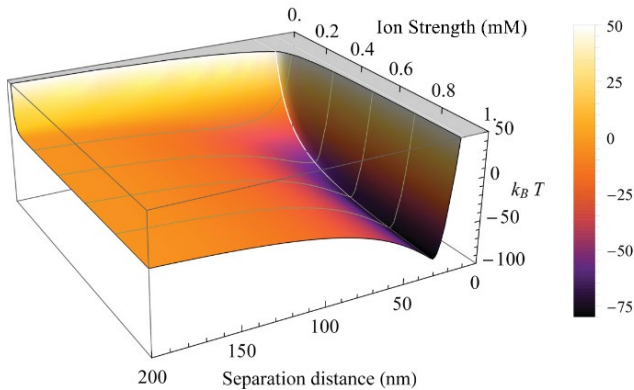


Fig. 10. Total interaction energy of SA-S-NZVI at different ionic strengths.

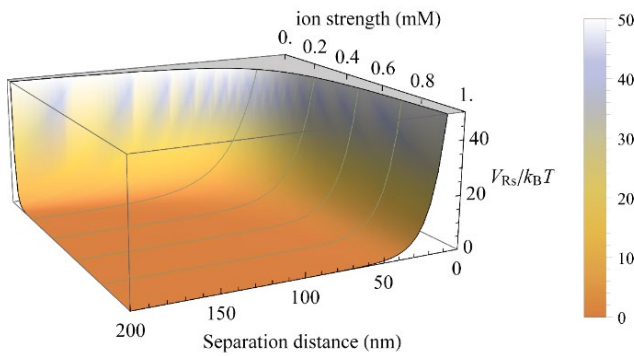


Fig. 11. Electrostatic potential energy of SA-S-NZVI at different ionic strengths.

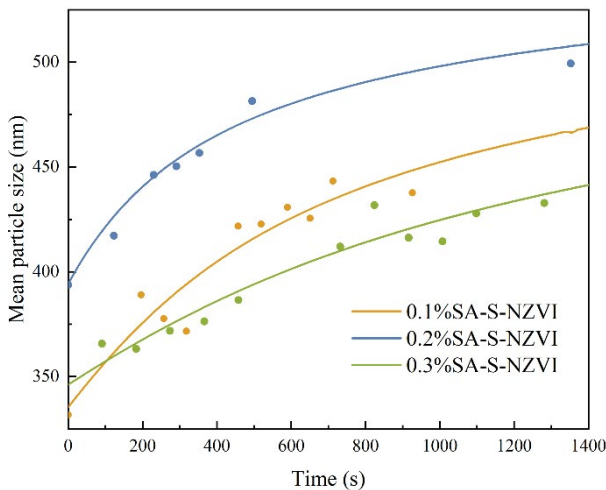


Fig. 12. Average particle size as a function of time.

to agglomerate due to the magnetic effect of S-NZVI. Bare S-NZVI has no repulsive potential barriers present, so irreversible aggregation occurs, and dense agglomerates should be formed.

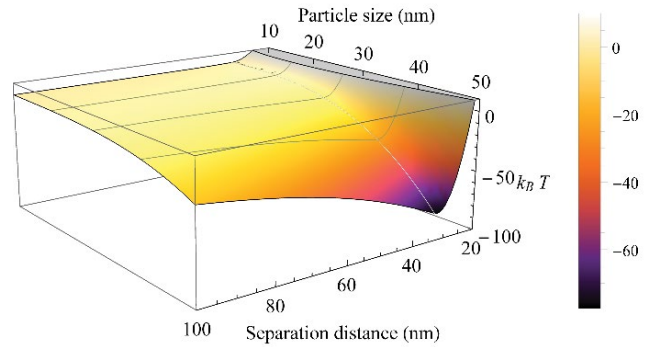


Fig. 13. Total XDLVO interaction energy of SA-S-NZVI at different particle sizes.

In contrast, SA-S-NZVI forms loose agglomerates of 31 nm instead of dense agglomerates of bare S-NZVI. In addition, although the small particles below 30 nm tend to agglomerate, the magnitude of the attraction potential energy is much smaller than the Brownian motion energy, which makes it difficult to form stable agglomerates. The magnetic effect of S-NZVI decays slowly with the increase of particle spacing, and the increase of electrostatic repulsion and spatial force can only achieve the repulsion at short distances. However, it cannot avoid the tendency of particles to approach each other at long distances. The magnetic interaction of S-NZVI decays slowly with increasing particle spacing. The magnetic properties of S-NZVI can be further improved by weakening the magnetic properties of S-NZVI or adding repulsive long-range forces to the system to match the magnetic range. This study has a great significance effect on the sedimentation process of water treatment, the problem of filter clogging of drinking water, and the problem of aquifer blockage in the infiltration process of surface water.

Acknowledgments

This work is supported by the Integration and demonstration of the technology research and development of Beijing Tianjin Hebei water resources security protection technology (2016YFC0401404). National key research and development program in 2016.

References

- [1] O. Falyouna, I. Maamoun, K. Bensaida, A. Tahara, Y. Sugihara, O. Eljamal, Encapsulation of iron nanoparticles with magnesium hydroxide shell for remarkable removal of ciprofloxacin from contaminated water, *J. Colloid Interface Sci.*, 605 (2022) 813–827.
- [2] R. Eljamal, I. Kahraman, O. Eljamal, I.P. Thompson, I. Maamoun, G. Yilmaz, Impact of nzvi on the formation of aerobic granules, bacterial growth and nutrient removal using aerobic sequencing batch reactor, *Environ. Technol. Innovation*, 19 (2020) 100911, doi: 10.1016/j.eti.2020.100911.
- [3] G. Vilardi, N. Verdone, Production of metallic iron nanoparticles in a baffled stirred tank reactor: optimization via computational fluid dynamics simulation, *Particuology*, 52 (2020) 83–96.
- [4] G. Vilardi, M. Stoller, L. Di Palma, K. Boodhoo, N. Verdone, Metallic iron nanoparticles intensified production by spinning disk reactor: optimization and fluid dynamics modelling,

- Chem. Eng. Process. Process Intensif., 146 (2019) 107683, doi: 10.1016/j.cep.2019.107683.
- [5] G. Vilardi, N. Verdona, R. Bubbico, Combined production of metallic-iron nanoparticles: exergy and energy analysis of two alternative processes using hydrazine and nabh₄ as reducing agents, *J. Taiwan Inst. Chem. Eng.*, 118 (2021) 97–111.
 - [6] S. Takami, O. Eljamal, A.M.E. Khalil, R. Eljamal, N. Matsunaga, Development of continuous system based on nanoscale zero valent iron particles for phosphorus removal, *J. JSCE*, 7 (2019) 30–42, doi: 10.2208/journalofjsce.7.1_30.
 - [7] R. Mokete, O. Eljamal, Y. Sugihara, Exploration of the reactivity of nanoscale zero-valent iron (NZVI) associated nanoparticles in diverse experimental conditions, *Chem. Eng. Process. Process Intensif.*, 150 (2020) 107879, doi: 10.1016/j.cep.2020.107879.
 - [8] T. Shubair, O. Eljamal, A. Tahara, Y. Sugihara, Preparation of new magnetic zeolite nanocomposites for removal of strontium from polluted waters, *J. Mol. Liq.*, 288 (2019) 111026, doi: 10.1016/j.molliq.2019.111026.
 - [9] I. Maamoun, O. Eljamal, O. Falyouna, R. Eljamal, Y. Sugihara, Stimulating effect of magnesium hydroxide on aqueous characteristics of iron nanocomposites, *Water Sci. Technol.*, 80 (2019) 1996–2002.
 - [10] F. He, Z. Li, S. Shi, W. Xu, H. Sheng, Y. Gu, Y. Jiang, B. Xi, Dechlorination of excess trichloroethene by bimetallic and sulfidated nanoscale zero-valent iron, *Environ. Sci. Technol.*, 52 (2018) 8627–8637.
 - [11] Y. Han, W. Yan, Reductive dechlorination of trichloroethene by zero-valent iron nanoparticles: reactivity enhancement through sulfidation treatment, *Environ. Sci. Technol.*, 50 (2016) 12992–13001.
 - [12] L. Zhou, T.L. Thanh, J. Gong, J.-H. Kim, E.-J. Kim, Y.-S. Chang, Carboxymethyl cellulose coating decreases toxicity and oxidizing capacity of nanoscale zero-valent iron, *Chemosphere*, 104 (2014) 155–161.
 - [13] M.A. Asad, U.T. Khan, M.M. Krol, Subsurface transport of carboxymethyl cellulose (CMC)-stabilized nanoscale zero valent iron (nZVI): numerical and statistical analysis, *J. Contam. Hydrol.*, 243 (2021) 103870, doi: 10.1016/j.jconhyd.2021.103870.
 - [14] W. Liu, J. Bai, Z. Chi, L. Ren, J. Dong, An in-situ reactive zone with xanthan gum modified reduced graphene oxide supported nanoscale zero-valent iron (XG-nZVI/rGO) for remediation of Cr(VI)-polluted aquifer: dynamic evolutions of Cr(VI) and environmental variables, *J. Environ. Chem. Eng.*, 9 (2021) 104987, doi: 10.1016/j.jece.2020.104987.
 - [15] A.K. Saha, A. Sinha, S. Pasupuleti, Modification, characterization and investigations of key factors controlling the transport of modified nano zero-valent iron (nZVI) in porous media, *Environ. Technol.*, 40 (2019) 1543–1556.
 - [16] H. Ohshima, *Theory of Colloid and Interfacial Electric Phenomena*, Elsevier, 2006.
 - [17] H. Ohshima, Electrokinetic phenomena of soft particles, *Curr. Opin. Colloid Interface Sci.*, 18 (2013) 73–82.
 - [18] S.K. Maurya, S. Sarkar, H.K. Mondal, H. Ohshima, P.P. Gopmandal, Electrophoresis of soft particles with hydrophobic inner core grafted with pH-regulated and highly charged polyelectrolyte layer, *Electrophoresis*, 43 (2022) 757–766.
 - [19] H. Ohshima, Electrostatic interaction of soft particles, *Adv. Colloid Interface Sci.*, 226 (2015) 2–16.
 - [20] H. Ohshima, Electrophoresis of soft particles, *Adv. Colloid Interface Sci.*, 62 (1995) 189–235.
 - [21] Q. Yu, J. Guo, Y. Muhammad, Q. Li, Z. Lu, J. Yun, Y. Liang, Mechanisms of enhanced hexavalent chromium removal from groundwater by sodium carboxymethyl cellulose stabilized zero-valent iron nanoparticles, *J. Environ. Manage.*, 276 (2020) 111245, doi: 10.1016/j.jenvman.2020.111245.
 - [22] T. Phenrat, N. Saleh, K. Sirk, R.D. Tilton, G.V. Lowry, Aggregation and sedimentation of aqueous nanoscale zero-valent iron dispersions, *Environ. Sci. Technol.*, 41 (2007) 284–290.
 - [23] D. Fan, G.O. Johnson, P.G. Tratnyek, R.L. Johnson, Sulfidation of nano zero-valent iron (nZVI) for improved selectivity during in-situ chemical reduction (ISCR), *Environ. Sci. Technol.*, 50 (2016) 9558–9565.
 - [24] Y. Li, Y. Zhang, Q. Jing, Y. Lin, The influence of Pluronic F-127 modification on nano zero-valent iron (nZVI): sedimentation and reactivity with 2,4-dichlorophenol in water using response surface methodology, *Catalysts*, 10 (2020) 412, doi: 10.3390/catal10040412.
 - [25] Y. Liu, Y.X. Zhang, S.S. Lan, S. Hou, Migration experiment and numerical simulation of modified nanoscale zero-valent iron (nZVI) in porous media, *J. Hydrol.*, 579 (2019) 124193.
 - [26] S.R.C. Rajajayavel, S. Ghoshal, Enhanced reductive dechlorination of trichloroethylene by sulfidated nanoscale zero-valent iron, *Water Res.*, 78 (2015) 144–153.
 - [27] K.L. Chen, M. Elimelech, Influence of humic acid on the aggregation kinetics of fullerene (C₆₀) nanoparticles in monovalent and divalent electrolyte solutions, *J. Colloid Interface Sci.*, 309 (2007) 126–134.
 - [28] K.L. Chen, S.E. Mylon, M. Elimelech, Aggregation kinetics of alginate-coated hematite nanoparticles in monovalent and divalent electrolytes, *Environ. Sci. Technol.*, 40 (2006) 1516–1523.
 - [29] K.L. Chen, M. Elimelech, Aggregation and deposition kinetics of fullerene (C₆₀) nanoparticles, *Langmuir*, 22 (2006) 10994–11001.
 - [30] H. Ohshima, Chapter 14 – General Expressions for the Force and Potential Energy of the Double Layer Interaction Between Two Charged Colloidal Particles and Analytic Approximations for the Interaction Between Two Parallel Plates, H. Ohshima, Ed., *Theory of Colloid and Interfacial Electric Phenomena*, Interface Science and Technology, Vol. 12, Elsevier, 2006, pp. 315–363.
 - [31] H. Ohshima, M. Nakamura, T. Kondo, Electrophoretic mobility of colloidal particles coated with a layer of adsorbed polymers, *Colloid Polym. Sci.*, 270 (1992) 873–877.
 - [32] M.V. Smoluchowski, Versuch einer mathematischen theorie der koagulationskinetik kolloider losungen, *Z. Phys. Chem.*, 92 (1917) 129–168.
 - [33] J. Škvarla, J. Škvarla, A unified analysis of the coagulation behaviour of silica hydrosols—when the colloid and polymer science meet, *Colloid Polym. Sci.*, 298 (2020) 123–138.
 - [34] H. Ohshima, M. Nakamura, T. Kondo, Electrophoretic mobility of colloidal particles coated with a layer of adsorbed polymers, *Colloid Polym. Sci.*, 270 (1992) 873–877.
 - [35] J. Gregory, Approximate expressions for retarded van der waals interaction, *J. Colloid Interface Sci.*, 83 (1981) 138–145.
 - [36] S.-W. Bian, I.A. Mudunkotuwa, T. Rupasinghe, V.H. Grassian, Aggregation and dissolution of 4 nm ZnO nanoparticles in aqueous environments: influence of pH, ionic strength, size, and adsorption of humic acid, *Langmuir*, 27 (2011) 6059–6068.
 - [37] K.A. Huynh, K.L. Chen, Aggregation kinetics of citrate and polyvinylpyrrolidone coated silver nanoparticles in monovalent and divalent electrolyte solutions, *Environ. Sci. Technol.*, 45 (2011) 5564–5571.
 - [38] M. Noh, T. Kim, H. Lee, C.-K. Kim, S.-W. Joo, K. Lee, Fluorescence quenching caused by aggregation of water-soluble CdSe quantum dots, *Colloids Surf., A*, 359 (2010) 39–44.
 - [39] H. Ohshima, Effective surface potential and double-layer interaction of colloidal particles, *J. Colloid Interface Sci.*, 174 (1995) 45–52.
 - [40] L. Wu, L. Liu, B. Gao, R. Muñoz-Carpena, M. Zhang, H. Chen, Z. Zhou, H. Wang, Aggregation kinetics of graphene oxides in aqueous solutions: experiments, mechanisms, and modeling, *Langmuir*, 29 (2013) 15174–15181.
 - [41] R. Bhardwaj, X. Fang, P. Somasundaran, D. Attinger, Self-assembly of colloidal particles from evaporating droplets: role of DLVO interactions and proposition of a phase diagram, *Langmuir*, 26 (2010) 7833–7842.
 - [42] L. Feriencikova, S. Xu, Deposition and remobilization of graphene oxide within saturated sand packs, *J. Hazard. Mater.*, 235 (2012) 194–200.
 - [43] K. Butter, P.H.H. Bomans, P.M. Frederik, G.J. Vroege, A.P. Philipse, Direct observation of dipolar chains in iron ferrofluids by cryogenic electron microscopy, *Nat. Mater.*, 2 (2003) 88–91.
 - [44] H. Ohshima, Chapter 16 – Double Layer Interaction Between Soft Particles, H. Ohshima, Ed., *Theory of Colloid and Interfacial*

Electric Phenomena, Interface Science and Technology, Vol. 12, Elsevier, 2006, pp. 390–408.

- [45] G. Fritz, V. Schädler, N. Willenbacher, N.J. Wagner, Electrosteric stabilization of colloidal dispersions, *Langmuir*, 18 (2002) 6381–6390.
- [46] J.L. Ortega-Vinuesa, A. Martín-Rodríguez, R. Hidalgo-Álvarez, Colloidal stability of polymer colloids with different interfacial

properties: mechanisms, *J. Colloid Interface Sci.*, 184 (1996) 259–267.

- [47] E. Piacenza, A. Presentato, R.J. Turner, Stability of biogenic metal(loid) nanomaterials related to the colloidal stabilization theory of chemical nanostructures, *Crit. Rev. Biotechnol.*, 38 (2018) 1137–1156.

Supplementary information

S1. Scanning electron microscopy analyses

Fig. S1 shows the scanning electron micrographs of the prepared S-NZVI coated with sodium alginate (SA-S-NZVI) with the selected magnification of 500,000–100,000 times. The synthesized SA-S-NZVI appeared spherical with about 50–100 nm diameter. The surface was wrapped by sodium alginate and well dispersed. The particles were stuck together in a chain-like arrangement by sodium alginate.

S2. Specific surface area determination

The specific surface area (SSA) of S-NZVI was determined using a fully automated specific surface area and pore size distribution analyzer (Nova Station C, Quantachrome Instruments). About 0.1 g of S-NZVI was weighed and degassed at 110°C for 3 h to remove water and other impurities and measured by nitrogen adsorption. The adsorption and desorption curves are shown in Fig. S2, and the specific surface area of S-NZVI was measured to be 36.248 m²/g.

S3. Mathematical calculation

S3.1. Calculation of collision frequency

The collision frequency function reflects the number of particle collisions per unit time in the dispersed system. In the aqueous environment, there are three main mechanisms of particle collisions: Brownian motion, fluid shear, and differential sedimentation [S1]. Using the Coalesced Fractal Sphere (CFS) model [S2]: (1) All flocs consist of a single type of primary particles, which are dense spheres. (2) All flocs have a fixed fractal dimension and are independent of the floc particle size. (3) When two flocs collide and combine, the newly formed flocs have the same fractal dimension as the pre-collision flocs, and the solid volume of the new flocs is the sum of the solid volumes of the pre-collision flocs. The three collision frequency functions β_{BR} , β_{SH} , β_{DS} for Brownian motion, fluid shear and differential sedimentation are calculated by the following equation [S2].

$$\beta_{BR}(v_i, v_j) = \frac{2k_B T}{3\mu} (v_i^{1/D_f} + v_j^{1/D_f}) (v_i^{-1/D_f} + v_j^{-1/D_f}) \quad (S1)$$

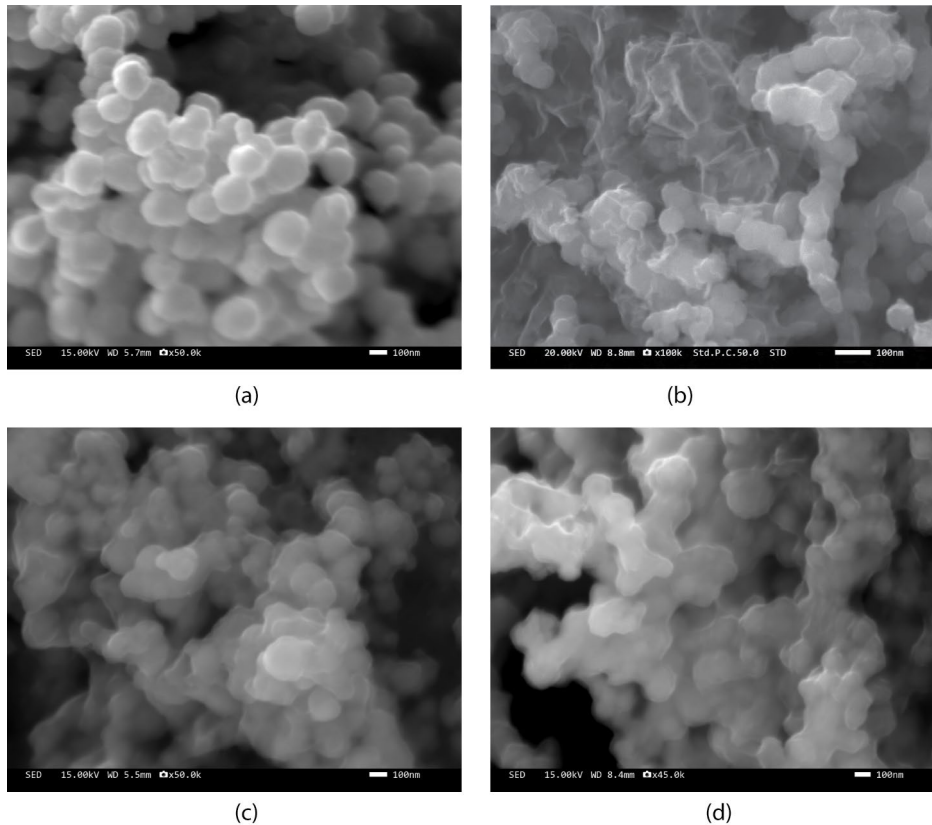


Fig. S1. Scanning electron microscopy images of (a) S-NZVI, (b) 0.1% SA-S-NZVI, (c) 0.2% SA-S-NZVI and (d) 0.3% SA-S-NZVI.

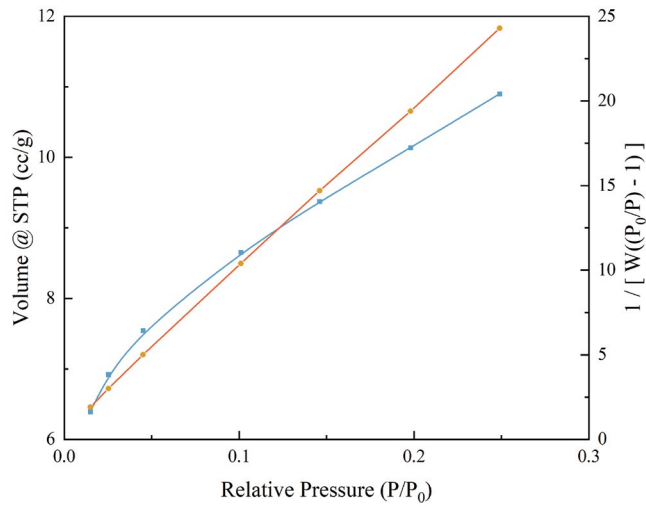
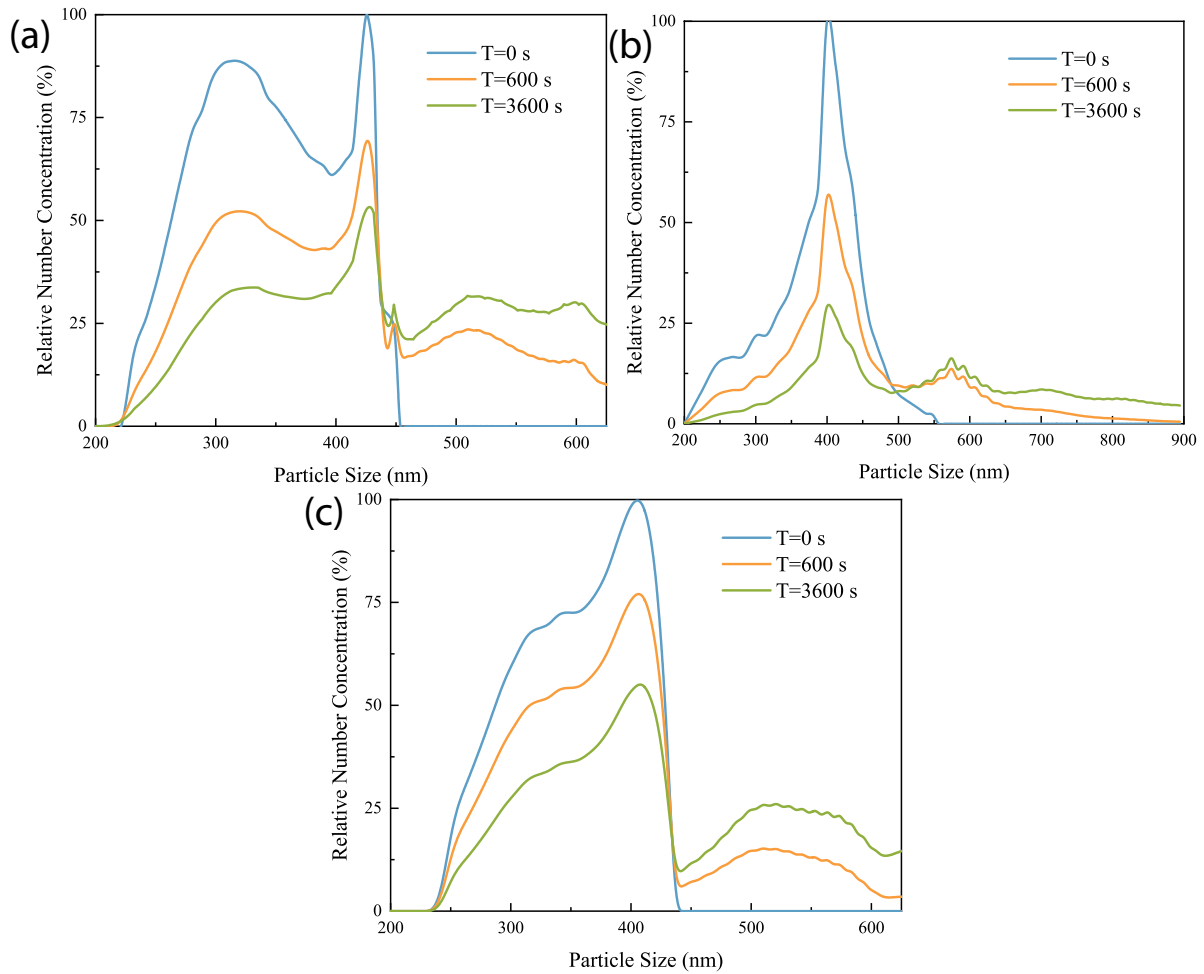


Fig. S2. Brunauer–Emmett–Teller test results

$$\beta_{\text{SH}}(v_i, v_j) = \frac{G}{\pi} v_0^{1-3/D_F} (v_i^{1/D_F} + v_j^{1/D_F})^3 \quad (\text{S2})$$

$$\beta_{\text{DS}}(v_i, v_j) = \begin{cases} \frac{g}{12\mu} \left(\frac{\pi}{6}\right)^{-1/3} [(\rho_0 - \rho_w)/\rho_w] v_0^{1/3-1/D_F} \\ \times (v_i^{1/D_F} + v_j^{1/D_F})^2 |v_i^{(D_F-1)/D_F} - v_j^{(D_F-1)/D_F}| & 2 \leq D_F \leq 3 \\ \frac{g}{12\mu} \left(\frac{\pi}{6}\right)^{-1/3} [(\rho_0 - \rho_w)/\rho_w] v_0^{4/3-3/D_F} \\ \times (v_i^{1/D_F} + v_j^{1/D_F})^2 |v_i^{1/D_F} - v_j^{1/D_F}| & 0 \leq D_F < 2 \end{cases} \quad (\text{S3})$$

where β (unit: $\text{m}^3 \text{s}^{-1}$) is the collision frequency function; v_0 (unit: m^3) is the particle volume, v_i and v_j are the solid volumes of different flocs, respectively; ρ_0 (unit: kg m^{-3}) is the monomer density; ρ_w (unit: kg m^{-3}) is the water density; D_F is the fractal dimension [3].

Fig. S3. Size distribution of particles in suspensions of 0.015 g L^{-1} (a) 0.1% SA-S-NZVI, (b) 0.2% SA-S-NZVI and (c) 0.3% SA-S-NZVI at different times.

S3.2. Determination of initial values

As shown in Fig. S3, the particle-size distribution at the moment of $T = 0$ was determined experimentally, and the Smoluchowski aggregation model was solved using this data as the initial condition. The scatter points were connected with Bessel curves for easy viewing. It can be seen that the initial hydraulic particle sizes of SA-S-NZVI with three cladding ratios were produced in the range of 200–500 nm for widely distributed samples. It should be noted that since the particle size of fresh solutions is mainly above 200 nm, the range during DLS testing of fresh solutions needs to be set to greater than 200 nm, ignoring the small amount of particles below 200 nm.

References

- [S1] D.N. Thomas, S.J. Judd, N. Fawcett, Flocculation modelling: a review, *Water Res.*, 33 (1999) 1579–1592.
- [S2] D.G. Lee, J.S. Bonner, L.S. Garton, A.N.S. Ernest, R.L. Autenrieth, Modeling coagulation kinetics incorporating fractal theories: a fractal rectilinear approach, *Water Res. (Oxford)*, 34 (2000) 1987–2000.
- [S3] Y. Liu, Y.X. Zhang, S.S. Lan, S.K. Hou, Migration experiment and numerical simulation of modified nanoscale zero-valent iron (nZVI) in porous media, *J. Hydrol.*, 579 (2019) 124193.